



Article

Hindcast and Near Real-Time Monitoring of Green Macroalgae Blooms in Shallow Coral Reef Lagoons Using Sentinel-2: A New-Caledonia Case Study

Maële Brisset ^{1,*}, Simon Van Wynsberge ¹, Serge Andréfouët ² , Claude Payri ², Benoît Soulard ¹, Emmanuel Bourassin ¹ , Romain Le Gendre ¹ and Emmanuel Coutures ³

¹ Institut Français de Recherche pour l'Exploitation de la Mer, UMR 9220 ENTROPIE (Institut de Recherche pour le Développement, Université de la Réunion, IFREMER, Université de la Nouvelle-Calédonie, Centre National de la Recherche Scientifique), Nouméa 98800, New Caledonia; Simon.Van.Wynsberge@ifremer.fr (S.V.W.); benoit.soulard@ifremer.fr (B.S.); Emmanuel.Bourassin@ifremer.fr (E.B.); rlegendr@ifremer.fr (R.L.G.)

² Institut de Recherche pour le Développement, UMR 9220 ENTROPIE (Institut de Recherche pour le Développement, Université de la Réunion, IFREMER, Université de la Nouvelle-Calédonie, Centre National de la Recherche Scientifique), BP A5, Nouméa CEDEX 98848, New Caledonia; serge.andrefouet@ird.fr (S.A.); claude.payri@ird.fr (C.P.)

³ Direction du Développement Durable des Territoires, Province Sud, Nouméa 98849, New Caledonia; emmanuel.coutures@province-sud.nc

* Correspondence: maele.brisset@ifremer.fr



Citation: Brisset, M.; Van Wynsberge, S.; Andréfouët, S.; Payri, C.; Soulard, B.; Bourassin, E.; Gendre, R.L.; Coutures, E. Hindcast and Near Real-Time Monitoring of Green Macroalgae Blooms in Shallow Coral Reef Lagoons Using Sentinel-2: A New-Caledonia Case Study. *Remote Sens.* **2021**, *13*, 211. <https://doi.org/10.3390/rs13020211>

Received: 26 November 2020

Accepted: 23 December 2020

Published: 9 January 2021

Publisher's Note: MDPI stays neutral with regard to jurisdictional claims in published maps and institutional affiliations.



Copyright: © 2021 by the authors. Licensee MDPI, Basel, Switzerland. This article is an open access article distributed under the terms and conditions of the Creative Commons Attribution (CC BY) license (<https://creativecommons.org/licenses/by/4.0/>).

Abstract: Despite the necessary trade-offs between spatial and temporal resolution, remote sensing is an effective approach to monitor macroalgae blooms, understand their origins and anticipate their developments. Monitoring of small tropical lagoons is challenging because they require high resolutions. Since 2017, the Sentinel-2 satellites has provided new perspectives, and the feasibility of monitoring green algae blooms was investigated in this study. In the Poé-Gouaro-Déva lagoon, New Caledonia, recent *Ulva* blooms are the cause of significant nuisances when beaching. Spectral indices using the blue and green spectral bands were confronted with field observations of algal abundances using images concurrent with fieldwork. Depending on seabed compositions and types of correction applied to reflectance data, the spectral indices explained between 1 and 64.9% of variance. The models providing the best statistical fit were used to revisit the algal dynamics using Sentinel-2 data from January 2017 to December 2019, through two image segmentation approaches: unsupervised and supervised. The latter accurately reproduced the two algal blooms that occurred in the area in 2018. This paper demonstrates that Sentinel-2 data can be an effective source to hindcast and monitor the dynamics of green algae in shallow lagoons.

Keywords: *Ulva*; Sentinel-2; satellite; remote sensing; algal bloom; coral reefs; Pacific lagoons

1. Introduction

Green tides, or massive blooms of green macroalgae that wash up on the shores, have spread around the world over the past decades, sometimes leading to significant economic, health and ecologic impacts [1,2]. Among the most significant events recorded are green tides in European locations such as Brittany and Venice Lagoon and in several Iberian estuaries [3–6]. They are also reported in the Yellow Sea on Chinese coasts [7] and in the Southeast Gulf of California in North America [8].

Green tides of macroalgae result from an excessive growth and proliferation (blooms) of competitive algae, usually from *Ulva* and *Cladophora* genera, when inorganic nutrients exceed the assimilative capacity of the surrounding ecosystem [9]. Algae biomass accumulations along coastlines, and their mats washed ashore, impact human activities and tourism. Beach cleaning and protection represent a significant cost and are not always

possible [10]. The proliferation of macroalgae also disturbs the equilibrium of coastal ecosystems, both temperate and tropical, via light reduction and via macroalgae decomposition that may generate anoxic conditions and hypoxia [11–13]. Beyond ecological damage, the accumulation of macroalgae biomass along coastlines can release hydrogen sulfide (H₂S) when decomposing under anoxic conditions, which may represent a serious risk for human and animal health.

To prevent or limit the impacts of green tides on society and ecosystems, some of the regions highly impacted by these events have developed expertise in risk assessment. Specifically, methods for monitoring and mapping macroalgae blooms were developed to understand their origin and attempt to anticipate mass beaching. Among the methods that have already been implemented are remote sensing approaches (see Scanlan et al., 2007 [14], for a review of existing strategies). Remote sensing studies carried out to monitor macroalgae focused on emerged or washed-ashore algae patterns (e.g., green tides in Brittany [15]), and on floating, rafting mats (e.g., [16–20]). Specifically, satellite imagery acquired at high temporal resolution (1 to 15 days) has allowed the detection of episodic blooms and provides pictures of these events which are spatially more representative than those provided by an often limited in situ number of stations and transects [14]. Furthermore, satellite archive data can be used to track the dynamic of algal blooms and identify their origins [17–21]. Ultimately, at high temporal resolution, images can be used to detect blooms in near real-time and predict their trajectory to assist the management of beach stranding events [22,23]. The main sensors used so far for these approaches were the Geostationary Ocean Color Imager (GOCI) at 500-m spatial resolution and 1 h revisit time [17,20,22,23]; the Moderate Resolution Imaging Spectroradiometer (MODIS) at 1200-m spatial resolution and 1 day revisit time [17,19–21]; the Ocean and Land Color Instrument (OLCI) at 300-m spatial resolution and 2 days revisit time [20]; the Wide Field of view (WFOV) at 16-m spatial resolution and 4 days revisit time [20]; and the Ocean Land Imager (OLI) at 30-m spatial resolution and 16 days revisit time [17,20].

Green tides can occur in small tropical lagoons where they often originate from algal biomass growing on the lagoon floor. When becoming unattached, they form blooms of loose or drift macroalgae. Proliferations are limited in sizes according to the lagoon scale, but they still create nuisances. Green algal blooms that develop in oligotrophic lagoons are much smaller in size compared to those recorded in eutrophic waters and, therefore, require higher spatial resolution satellite imagery to be detected. High revisit frequency satellites (i.e., ~1 day) have the temporal resolution suitable to monitor blooms in these ecosystems, but their spatial resolution (i.e., ≥ 100 m) is too coarse for the lagoon and algal mats dimensions to provide accurate estimates. Bloom monitoring in small lagoons ideally requires both high temporal and spatial resolutions and, ideally, at low cost. Satellites with Very High Spatial Resolution (VHR, i.e., < 4 m) are suitable to detect fine spatial features, but their on-request tasking procedures have a significant cost and can prevent real-time monitoring. An overview of existing sensors suggests that few sensors provide adequate capacities. Several studies have shown the potential of VHR satellite imagery to map and estimate long term biomass of macroalgae in shallow lagoons [24–26], but they did not focus on green algae. These studies also show that these recent satellite missions provide limited temporal coverage to hindcast the blooms of macroalgae, which can be very episodic.

In 2014, the European Space Agency (ESA) started the Copernicus program and launched the two Sentinel-2 satellites, which supply since 2017 free data at 10-m resolution with a 5-day revisiting time. The Multi Spectral Instrument (MSI) used for this program offers an interesting trade-off between cost and spatial and temporal resolutions that should be more suitable than previous remote sensing commercial products for characterizing the dynamics of green algae blooms in tropical lagoons. Thus, Sentinel-2 brings new perspectives to monitor these events. Here, we tested the ability of Sentinel-2 imagery to characterize green macroalgae dynamics within a shallow coral reef lagoon in New Caledonia recently impacted by green tides. First, using images quasi-concurrent with

field data, we fitted a relationship between in situ algal abundance and various radiometric indices calculated from Sentinel-2 MSI reflectances. Then, the best model was used to extrapolate algal dynamics over a three-year period, from January 2017 to December 2019. The method has been evaluated regarding its ability in capturing two documented *Ulva* spp. blooms that occurred in 2018 and 2019 in the studied area [27,28].

2. Materials and Methods

2.1. Study Site

New Caledonia is a French overseas territory, located in the south-western Pacific Ocean, ~1500 km east of Australia (Figure 1a). It comprises one main large island, known as Grande Terre, bordered by a 1600-km long barrier reef, which delimits a 23,400 km² lagoon [29]. Due to their good health conditions and high biodiversity, six different areas, or clusters, of New Caledonia reefs and lagoons were listed as UNESCO World Heritage Areas in 2008 [30]. New Caledonia is not spared from green tides, with occasional events of short duration recorded since 1996 in the bays near the town of Nouméa, and induced by the Japanese algae *Ulva ohnoi*.

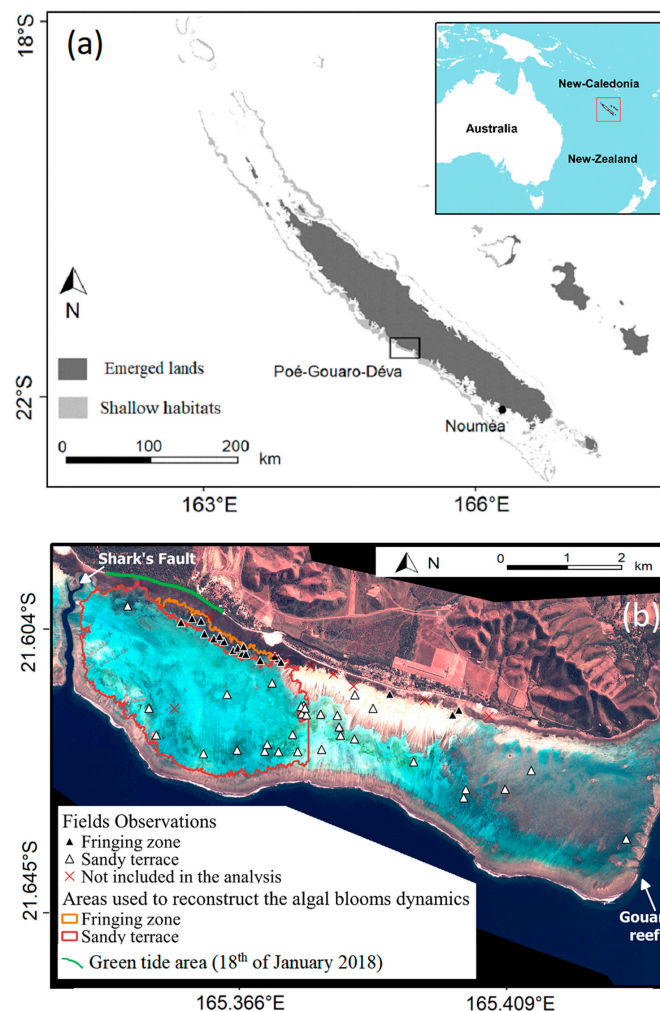


Figure 1. Study site description. (a) Geographical location of the Poé-Gouaro-Deva (PGD) area on New Caledonia's main island, Grande Terre. The shallow habitat layer is from the Millennium Coral Reef Mapping Project [31]. (b) Location of field observations and boundaries of the two areas considered in this study to reconstruct the green algal dynamics, namely the fringing zone and the sandy terrace. The image shown here is a very high-resolution Pléiades remote sensing image from 17 July 2017, used to select field sampling stations (see Section 2.2).

The present study focuses on the Poé-Gouaro-Deva (PGD) zone (21°37'10"S, 165°23'16"E) located on the west coast of Grande Terre. The studied area is located on the coastal area in the Bourail region, in the South Province of New Caledonia. It is bounded by the Gouaro reef in the southeast, and by the so-called Shark's Fault (Faille aux requins) in the northwest. The area contains a Marine Protected Area (MPA) and is included in the UNESCO areas. The coral reef complex borders the coastline (Figure 1b), forming a narrow (<3 km) and shallow lagoon (maximum depth ~4 m). Tides in this area can be classified as micro-tidal, mixed and mainly semi-diurnal, with a tidal range that can reach a maximum of 1.8 m during spring tide. The northwest part of the lagoon (~10 km²) is mainly made of sandy soft-bottom habitat, while the southeast part (~9 km²) is dominated by hard ground and coral communities and patch reefs. A several tens of meters-wide fringing seagrass bed (~3 km²) borders the shoreline [31]. This seagrass belt is not homogeneous and can be intertwined with patch of coral communities (branching *Montipora* and *Acropora*) and sand.

The PGD area is a hotspot of tourism activities, with increasing human pressures on the reef and lagoon ecosystems. Tourist frequentation has increased over recent years, with about 4000 Deva visitors in 2017 and more than 6500 in 2019 (data from Maison de Deva). Developing lands have also tripled in surface area from 1998 (~100 ha) to 2014 (~350 ha, [32]). In early 2018, a green tide occurred in the PGD lagoon, with green macroalgae washed onshore in significant amounts on 18 January (~500 m³ collected in three clean-up operations, Coutures personal observations), mostly along a 2.5-km long coastline located in the northwest part of the study zone (Figure 1b). The algae decaying on the beach prevented tourism activities and could induce health threats. Another stranding event, although of a smaller intensity than the first event, impacted the beach on 1 June 2019.

2.2. In Situ Measurements of Algal Abundance

Field investigations were first carried out in February 2019 and May 2019, at 24 and 42 stations, respectively. Among the 24 stations visited in February 2019, most of them were revisited in May 2019. All stations were preliminarily selected using a remote sensing-driven site selection method, similar to that in Andréfouët and Wantiez (2010) [33], to best capture the diversity of habitat in the area (seagrass bed, sand, coral reef and mixed habitats). For station selection, we used a multispectral Pléiades image ([34], Airbus DS Geo distribution, resolution ~70 cm) dated from 17 July 2017.

Second, three field trips took place in July 2019, September 2019 and November 2019, with a sampling dedicated to the monitoring of one single station (B21) where the biomass observed in February and May was particularly high (Figure 2a, Figure 3b).



Figure 2. Variation in green algae cover observed in the Poé-Gouaro-Déva lagoon during the study. (a) Algal cover observed in May 2019, in the fringing area (abundance index $I_a = 5$); (b) and (c) algal cover observed in May 2019, in the sandy terrace (abundance index $I_a = 3$ and $I_a = 1$, respectively).

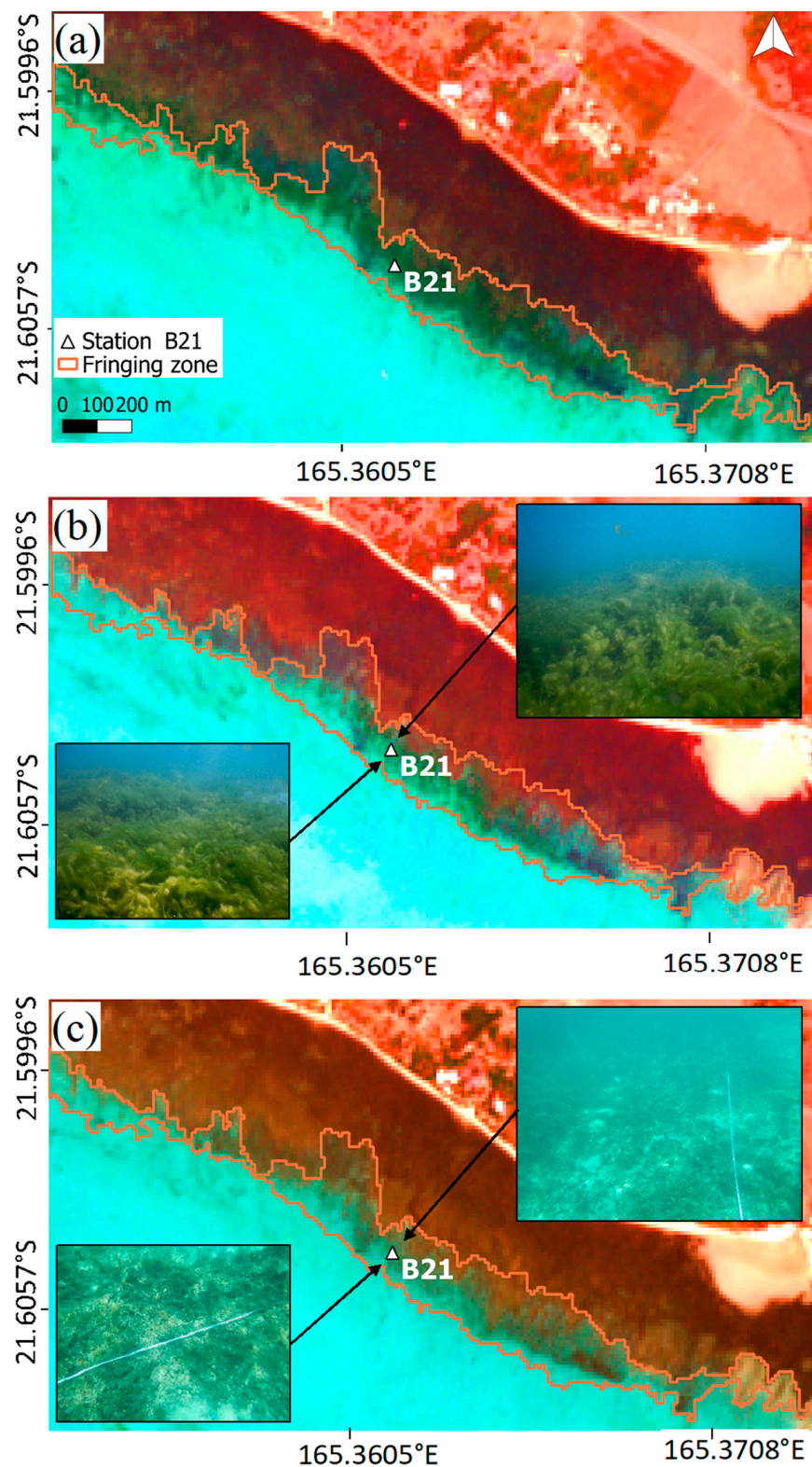


Figure 3. Correspondence between the Sentinel-2 images and the abundance of green algae in the fringing area (a) just before the January 2018 green tide (Sentinel-2 image dated from 4 January 2018), (b) during high biomass period (Sentinel-2 image dated from 13 February 2019, photographs at station B21 from 20 February 2019) and (c) during low abundance period (Sentinel-2 reference image from 25 November 2019 and photographs at station B21 from 18 November 2019).

Finally, 11 new additional stations were opportunistically sampled during 4 surveys dedicated to seawater samplings in December 2018, March 2019, July 2019 and October 2019. These stations did not specifically target areas with known past high abundances of green algae.

For each survey and each station, the cover of green algae was estimated semi-quantitatively using the Braun-Blanquet cover-abundance scale [35], ranging from 0 (no green algae) to 5 (cover exceeding 75%) from wide-angle photos and videos taken during the field investigations (Table 1; Figure 2). The method is similar to the Medium-Scale Approach [36] used to describe fish habitats using a semi-qualitative scale for each benthic descriptor. The results are estimates of green algae abundance (index \bar{I}_a) at a scale compatible with the resolution of Sentinel-2 data (100 m² pixels, see next section). In total, 9 samplings campaigns carried out from December 2018 to November 2019 provided 97 measurements of green algae abundances, with 57 along the fringing and seagrass reef and 40 spread over the sandy terrace (Figure 1b). This method was favored compared to a quantitative approach (using transects or quadrats) because it allows for covering a large area with more stations. Although this approach provided less precise estimates of algae abundance for each pixel individually, it could survey a large panel of pixels in different configurations.

Table 1. Semi-quantitative index (I_a) used in this study to quantify green algae abundance, based on the Braun-Blanquet index of abundance dominance [35].

I_a	Green Algae Cover (%)
0	<1
1	1–5
2	5–25
3	25–50
4	50–75
5	>75

2.3. Sentinel-2 Data Sets

Cloud-free Sentinel-2 images (10 m resolution) available for the study area were retrieved from the Data Hub website (© Data Hub System 2.4.1, [37]; Figure 4). Data downloads provided a time-series of images from 2017 to 2019. This consisted of Level 2A images (i.e., images corrected for the atmospheric signal) when available. Otherwise, Level 1C images (i.e., images without atmospheric correction) were used and were atmospherically corrected using the Sen2Cor processor from SNAP (© SNAP, 7.0) to create Level 2A products. This open-source program developed by the ESA provides surface, bottom of atmosphere (BOA) reflectance similar to the Level 2A products provided by the ESA/Copernicus program. Since we aim to apply statistical segmentation, classification and empirical correction to estimate algal abundance (see below), BOA reflectance was deemed adequate and no further correction was applied, for instance, to attempt to correct the air–water interface in the lagoon.

The Sentinel-2 MSI instrument measures reflected radiance in 13 spectral bands. Four of them have a 10-m spatial resolution, namely the blue (490 nm); green (560 nm); red (670 nm) and near-infrared (850 nm) bands. Only spectral bands in the blue ($B2$) and in the green ($B3$) zones were considered for this study, because red and especially near-infrared signals are attenuated quickly in the water column [38].

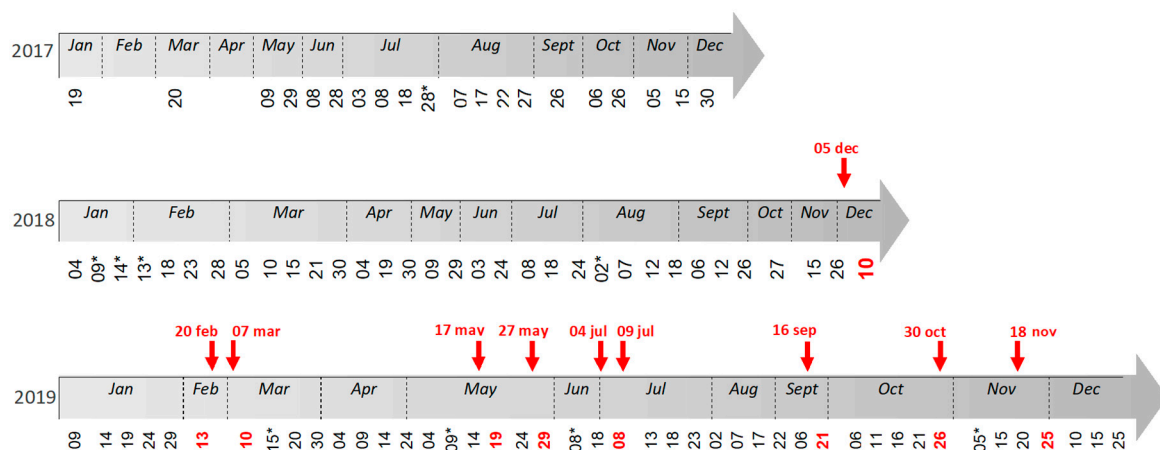


Figure 4. Historical timeline of the Sentinel-2 images downloaded from the Data Hub Copernicus website and used in this study. The dates annotated with ‘*’ are used for the fringing area only due to a significant cloud cover above the sandy terrace. The timeline associates the fieldwork dates (red arrows) to the dates of the Sentinel-2 images used to calibrate the model (red numbers).

Prior to performing a change detection analysis, two methods were implemented to empirically inter-calibrate BOA reflectance between images. These corrections used a Sentinel-2 image dated from 25 November 2019 as a radiometric reference because the concurrent field trip performed in this period (18 November 2019) highlighted a very low algal cover in the studied area (Figure 3c). At the time of the analysis, the 25 November 2019 image was the closest in time available to this field trip. The first method (hereafter named “type 1 correction”) is an empirical band-to-band and image-to-image correction which required identifying, across the time-series, 105 pixels considered as pseudo-invariant features on the ground. The method relies on the hypothesis that the targeted objects (e.g., roads and roofs) are radiometrically invariant during the studied period. Any instability in the reflectance of these objects, therefore, can create biases due to environmental conditions (e.g., wetness on ground) or noise at the time of processing after image acquisition (resampling). To inter-calibrate the images, a band-specific linear relationship was built between the BOA reflectances of the pseudo-invariant features for each pair of images (reference image and image to be processed) using Equations (1) and (2) [39].

$$R(B2)_{cor1} = a \times R(B2) + b \quad (1)$$

$$R(B3)_{cor1} = c \times R(B3) + d \quad (2)$$

where a , b , c and d are the coefficients of the linear relationships built from the pseudo-invariant pixels and $R(B2)$ and $R(B3)$, the BOA reflectances of the spectral bands in the blue and the green.

The second correction aimed at minimizing the differences caused by the seabed composition (other than green macroalgae) within an image. $B2$ and $B3$ reflectances associated to each pixel were standardized following Equations (3) and (4). This correction was first applied alone (hereafter named “type 2 correction”), and we also applied this correction followed by the first one (“type 3 correction”).

$$R(B2)_{cor2} = \left(\frac{R(B2)_{ref} - R(B2)}{R(B2)_{ref}} \right) + \overline{R(B2)_{ref}} \quad (3)$$

$$R(B3)_{cor2} = \left(\frac{R(B3)_{ref} - R(B3)}{R(B3)_{ref}} \right) + \overline{R(B3)_{ref}} \quad (4)$$

where $R(B2)_{ref}$ and $R(B3)_{ref}$ are the BOA reflectances in the blue and the green bands, respectively, associated to the reference image (25 November 2019); and $\overline{R(B2)_{ref}}$ and $\overline{R(B3)_{ref}}$ are the arithmetic means of reflectance across all pixels associated to the field stations of this image. These constants were added to avoid generating negative radiometric values, which are not compatible with the calculation of some of the radiometric indices (cf. next section).

Note that correcting for co-registration errors was not performed in our study since the L1C processing chain already implements a geometric step which aims at improving the repetitiveness of the image geolocation in order to reach a multi-temporal geolocation target (<0.5 pixel at 95% confidence). When performing the type 1 correction, we could further confirm that the set of Sentinel-2 images we used was affected by negligible co-registration errors, since locations of the pseudo-invariant pixels were stable, and no offset of these pixels over time could be noticed.

2.4. Relationship Between Reflectance and Green Algae Abundances

To calibrate a biomass vs. reflectance (or spectral index, see below) relationship, for each sampling campaign the analysis was performed on the closest Sentinel-2 image in time. Offset between field work and image acquisition was always inferior to 7 days (Figure 4). GPS measurements of the field stations were deemed precise at pixel resolution after comparison with remarkable features visible on ground and in images.

The blue and green BOA values were then used to compute six radiometric indices.

- Two mono-band indices (designated ρ_b and ρ_g) used either blue or green BOA values, with or without the correction types.
- Four multispectral additional indices (designated θ_1 to θ_4) were generated from different combinations of ρ_b and ρ_g , with or without the corrections (Equations (5)–(8)). These indices were inspired from spectral vegetation indices used in the literature, such as the Simple Ratio (SR) index for θ_1 [40,41], the Normalized Difference Vegetation Index (NDVI) for θ_2 [42], the Modified Simple Ratio (MSR) for θ_3 [43] and an attempt to combine the merits of NDVI and SR ($\text{NDVI} \times \text{SR}$) for θ_4 [44].

$$\theta_1 = \frac{\rho_g}{\rho_b} \quad (5)$$

$$\theta_2 = \frac{\rho_g - \rho_b}{\rho_g + \rho_b} \quad (6)$$

$$\theta_3 = \frac{\left(\frac{\rho_g}{\rho_b}\right) - 1}{\sqrt{\frac{\rho_g}{\rho_b} + 1}} \quad (7)$$

$$\theta_4 = \frac{\rho_g * (\rho_g - \rho_b)}{\rho_b * (\rho_g + \rho_b)} \quad (8)$$

For the two types of substratum encountered in the study area, namely sandy bottoms vs. mix substrates along the fringing area (made of unconsolidated calcareous and terrigenous sand, coral and seagrass), the semi-quantitative abundance of green algae from field observations was expressed as a function of each radiometric index, using a non-parametric smooth function calibrated via the R studio mgcv package (©2009–2019 R studio v1.2.1578). The performance of the models was compared on the basis of the percentage of variance explained and using the generalized cross-validation (GCV) criteria.

2.5. Mapping of Green Algal Dynamics

We hindcasted the dynamics of green algae over the period covered by the Sentinel-2 imagery (from 19 January 2017 to 12 December 2019) for two shallow areas of interest in the PGD area (Figure 1b). These areas were selected after field work considering they were

prone to macroalgae proliferation or accumulation. The first area (hereafter named ‘the fringing area’; ≈ 48 ha) included very shallow (<2-m depth at low tide) stations located along the littoral in the west part of the lagoon. It is characterized by a mosaic of benthic components (seagrass, sand and corals). The second area (hereafter named ‘the sandy terrace’; ≈ 780 ha) was also located in the west part of the lagoon but included stations located on the sandy terrace away from the littoral and in slightly deeper water (2–4 m deep at low tide).

For each area of interest, two different methods were tested to extrapolate the abundance of green algae. The first approach (hereafter ‘the unsupervised approach’) used the best fitted model selected in the previous section to predict, for each pixel located in the area of interest, the algal abundance (I_a) from the $R(B2)$ and $R(B3)$ radiometric values. This was realized using the `predict.gam` function with the R studio `mgcv` package. The reconstruction of green algae dynamics was performed for the two areas of interest, computing, for each area, the arithmetic mean value of algae abundance per pixel (\bar{I}_a) (Equation (9)).

$$\bar{I}_a = \frac{\sum_{i=1}^n I_{a_i}}{n} \quad (9)$$

where n refers to the number of pixels in the area of interest.

The second approach (hereafter ‘the supervised approach’) involves a photo interpretation step. First, the two areas of interest were segmented in order to define homogeneous polygons in terms of blue and green radiometric values. The segmentation was performed using the automatized meanshift algorithm of the Orfeo ToolBox (OTB) plugin from QGIS software (© Qgis version 3.10.4). Then, algal-free polygons were visually identified by one of the authors (M.B.) and dismissed from the analysis. For each remaining polygon, an abundance-dominance green algae index was predicted, following the same procedure as for the unsupervised approach. The reconstruction of green algae dynamics was performed by computing, for each area of interest, the arithmetic weighted mean value of algae abundance associated to each polygon (I_a), weighted by its surface area (Equation (10)).

$$\bar{I}_a = \frac{\sum_{i=1}^n (I_{a_i} \times A_i)}{\sum_{i=1}^n A_i} \quad (10)$$

where n refers to the number of polygons in the area of interest and A_i the surface area of polygon i .

The various time-series of green algae abundances (\bar{I}_a) obtained from the combination of different image inter-calibration procedures, spectral indices and mapping procedures were compared regarding their ability to reproduce the two green tides recorded in the study area in 2018 and 2019.

3. Results

3.1. Algal Diversity

Several species of green algae (Chlorophyta) have been observed in the different study areas in the lagoon, including *Boodlea*, *Chaetomorpha*, *Cladophora* and *Ulva*. *Ulva* was dominant, with several species having a filamentous and tubular morphology. A molecular taxonomical study currently being completed has shown the coexistence of four genetically different species. Three of them are attached to the substratum mainly in sandy areas, while the blooms consist of free-moving masses of strongly entangled filaments which accumulate along the coastline in the seagrass areas. The bloom-forming alga is a highly branched species of *Ulva* (*Ulva* sp3) which morphologically resembles *Ulva prolifera* but is genetically distinct from it. In some samples from the blooms, there could be several taxa (*Boodlea* and *Cladophora*), but most of the time, the dominant species was *Ulva* sp3.

3.2. In Situ Estimation of Algal Abundance

In February 2019, green algae were abundant ($2 < I_a < 5$) at two stations located in the fringing zone in the western part of the lagoon. Relatively high abundance-dominance indices ($2 < I_a < 3$) were also obtained for three stations on the sandy terrace. The abundance of algae was poor or null ($I_a \leq 1$) at all other stations. In May 2019, the spatial distribution of green algae was similar to February 2019, with abundance-dominance indices from 0 to 4 at stations located in the sandy terraces and from 0 to 5 at stations located in the fringing zone. Along this area, a significant variability in abundance ($0 < I_a < 5$) was also found between stations during all of the 2019 surveys, except in November 2019, when abundance was low ($I_a = 0$) all across the fringing zone.

The wide range of I_a values across the different field surveys and stations allowed for calibrating a representative and robust relationship between I_a and the radiometric indices derived from remote sensing images (see next section).

3.3. Relationship between Radiometric Indices and Algal Abundance

Without any correction applied (neither type 1, 2 nor 3), the multispectral indices θ_1 , θ_2 , θ_3 and θ_4 better explained variance than the ρ_b and ρ_g indices (Figure 5). This trend was obtained both for stations located in the fringing zone (i.e., between 48.6% and 50.3% of variance explained by θ_1 , θ_2 , θ_3 and θ_4 vs. 27.2% and 31.5% of variance explained by ρ_b and ρ_g) and for stations located in the sandy zone stations (i.e., 32.3–32.5% vs. 6% and 1%).

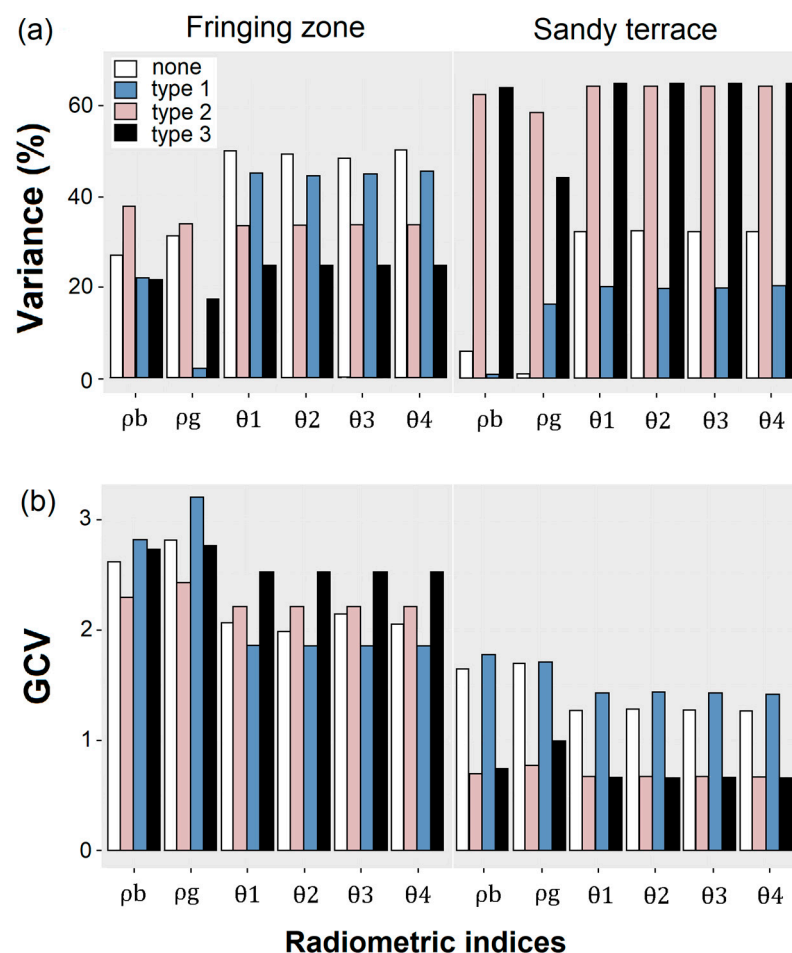


Figure 5. Performance of the fitted relationships between the green algae abundance and the radiometric indices, depending on the type of correction (type 1, type 2 or type 3). (a) Comparison of the relationships regarding the variance in algae abundance they explained. (b) Comparison of the relationships regarding the generalized cross-validation (GCV) criteria.

For the stations located on the sandy terrace, the type 2 and 3 corrections improved the goodness-of-fit test results (Figure 5). Specially for the $\theta 4$ index, the explained variance increased from 32.3% without correction to 64.3% with type 2 correction and to 64.9% with type 3 correction. However, applying the type 2 or the type 3 correction degraded the fit for the fringing zone (Figure 5).

Eventually, the $\theta 4$ index based on $R(B2)$ and $R(B3)$ without any corrections provided the best model for the fringing zone (i.e., 50.3% of variance, $GCV = 2.06$, Figure 6b). For the sandy terrace, $\theta 4$ also provided the best model (i.e., 64.9% of variance, $GCV = 0.66$, Figure 6a) but only when the type 3 correction was applied (Figure 5). These indices and correction types were therefore selected to extrapolate the algal abundance across the Sentinel-2 time-series (next section).

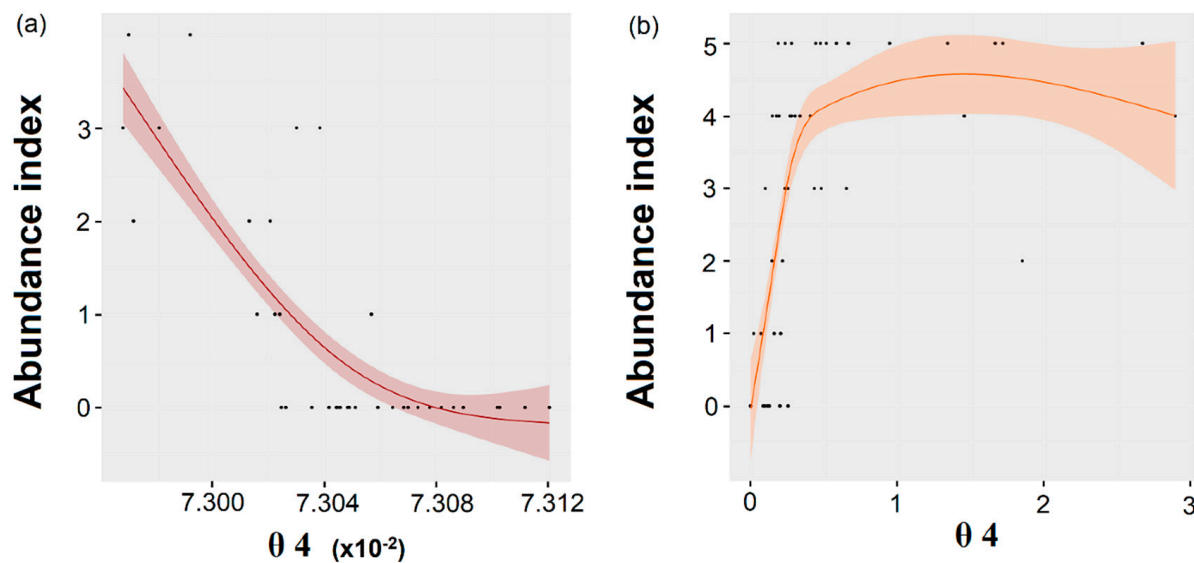


Figure 6. Calibration of a smooth function (non-parametric relationship) between the green algal abundance and the radiometric index $\theta 4$. (a) Fitted relationship for the stations located in the sandy terrace ($n = 40$; variance explained by the model = 64.9%; $GCV = 0.66$); radiance was corrected with type 3 correction. (b) Fitted relationship for the stations located in the fringing zone ($n = 57$; variance explained by the model = 50.3%; $GCV = 2.06$), without any radiance correction.

3.4. Mapping and Dynamics of Green Algae Abundances Using Sentinel-2

For the fringing area, using the supervised approach always yielded lower \bar{I}_a values than with the unsupervised approach ($\bar{I}_a = 0.63$ on average over the period of 2017–2019 against 2.00; Figure 7a). Despite this difference, both approaches could identify the January 2018 and June 2019 algal blooms, both producing significant macroalgae pile-ups on the beach. The abundance variations hindcasted on the sandy terrace area were not always synchronous with those hindcasted in the fringing area. Unlike the fringing zone, the supervised and unsupervised approaches were more in agreement to each other in this habitat (Figure 7b). The dynamics of green algae hindcasted for both areas by the supervised and unsupervised approaches suggested high algal abundance throughout the year, except during the dry season (October and November; Figure 7). In particular, periods of high algal abundance were predicted around July 2017, July 2018 and July 2019 for both fringing and sandy terrace areas, although no green tide was reported, to our knowledge, during these periods.

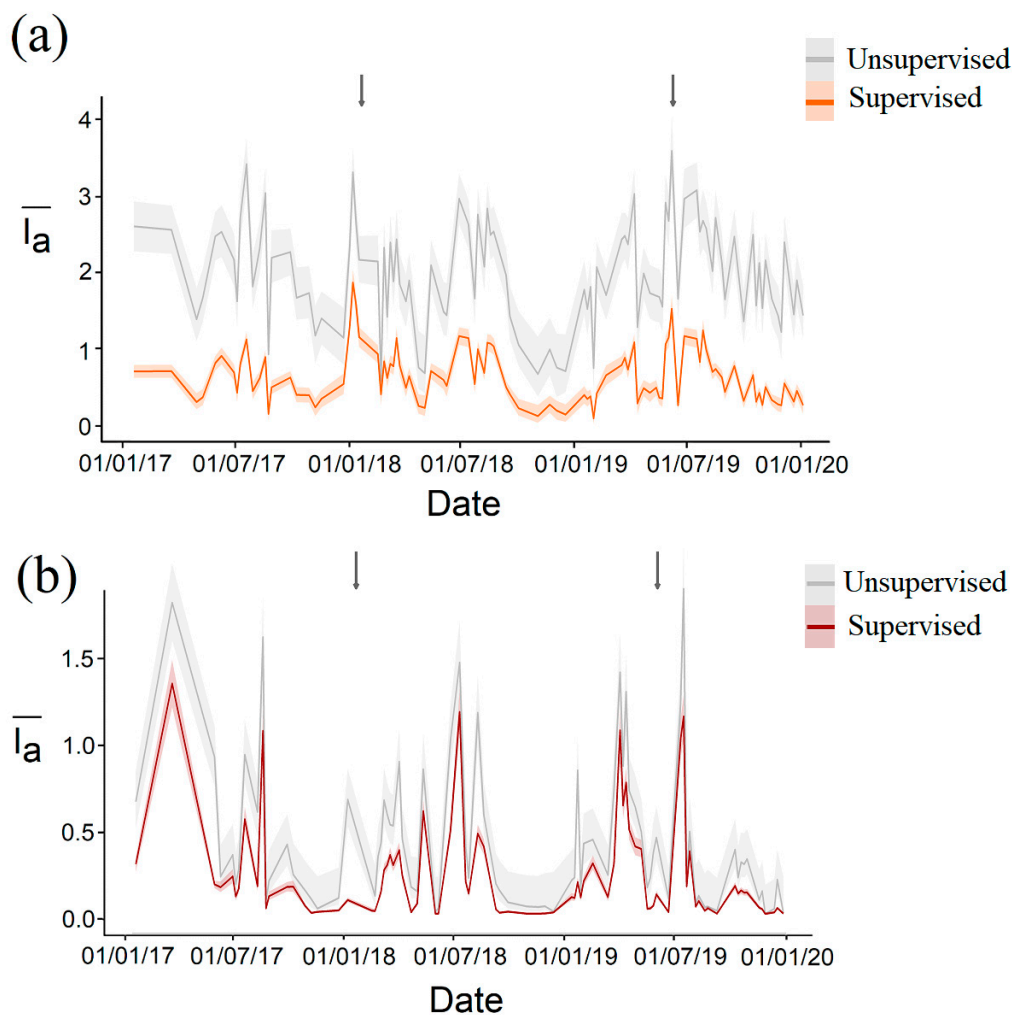


Figure 7. Variation in mean algal abundances (\bar{I}_a) over time, from 2017 to 2019, based on Sentinel-2 images, depending on the two different applied methodologies (unsupervised vs. supervised) (a) for the fringing area and (b) for the sandy terrace area. Arrows marks the dates of reported stranding events on the PGD beach.

4. Discussion

4.1. Innovative Nature of the Approach and Proposed Method

This paper demonstrates that the Sentinel-2 imagery is a valuable tool to hindcast the dynamics of benthic green algae in shallow coral reef lagoons, which is required to understand the causes of the algal tides when confronted with other data sets (e.g., lagoon temperature; solar irradiance; rainfall or streamflow from nearby rivers). Here, we focused on the benthic biomass of green macroalgae during blooming conditions in a shallow lagoon. This is in contrast with most recent remote sensing studies which looked at green and brown algae once they had beached and algal rafts while drifting on the ocean surface [16–21].

To date, most of the multispectral indices proposed in the literature for detecting macroalgae used the red visible and/or near-infrared bands [19,20,23,45–47]. These spectral bands have been commonly used because they are suitable to capture chlorophyll absorption peaks and the overall vegetation spectral signature when it is above water or just at the ocean surface. The NDVI, which uses a ratio of the red visible and near-infrared bands, has been widely used as an indicator of floating algae mats' presence/absence [20,48–50]. The NDVI has also been used successfully for mapping and monitoring phanerogams [51]. Despite the potential of the red and near-infrared bands to distinguish vegetation, these radiations are quickly attenuated in water, and spectral indices based on these bands are

very sensitive to depth variations, either due to bathymetry or tide [52,53]. For instance, Andréfouët et al. [26] showed that even in a low-depth environment (<2 m), red and near-infrared bands were not ideal to map the biomass of benthic *Sargassum polycystum* brown algae. Although the index of floating algae based on the red and near-infrared bands may be useful to identify the presence of green algae in their final floating cycle, this index was of low interest in our case study, because the floating phase of algae's life cycle is very short and was never observed during field work. This made NDVI a poor proxy of algal abundance in our case study (Figure S1). In this paper, a modified version of the NDVI, switching the red and infrared bands with blue and green bands, provided more conclusive results to quantify the abundance of benthic green algae. This agreed with previous studies that used NDVI-like indices with a variety of band combinations [53,54].

In our study, multispectral radiometric indices (i.e., θ_1 , θ_2 , θ_3 and θ_4) provided more convincing results than the green band alone (i.e., ρ_g). These findings are in contrast with the work of Andréfouët et al. [26] for *S. polycystum* in an atoll lagoon. For this brown alga, the green band provided a fit with biomass nearly as good as our multispectral indices and was used to hindcast its dynamics from 2002 to 2015 using a range of high-resolution remote sensing images (QuickBird 2, IKONOS, WorldView-2, Pléiades 1B, 1A).

4.2. Influence of the Three Types of Corrections

Using the type 1 empirical approach alone to correct the radiometric data was found to be of limited interest. Two explanations can be provided. First, our study relied on images that were corrected beforehand with an ESA model in order to remove the atmospheric signal. It implies that the additional type 1 correction provided no added value to monitor the green algal proliferation, compared to using L2A images. This might be the result of using imperfect pseudo-invariant features for this correction. However, models and algorithms automatically used to correct the entire L1C images are unlikely to be enough to perfectly correct the images locally in our studied areas of interest [55,56]. Specifically, for coral reef areas, local processes can affect the atmospheric signal quality, such as ocean spray induced by waves breaking on the reef ridge.

Secondly, previous studies already highlighted the limits of the type 1 correction for areas of high algal biomass. High biomass is correlated with low radiometric value (in the green band, or for a given radiometric index [26]). Indeed, in such a configuration, the relationship applied to estimate biomass is very sensitive because a wide range of biomass corresponds to a narrow radiometric range. However, the type 1 correction for intercalibrating images is easily applicable to coastal areas where remarkable pixels can be precisely identified in all the images acquired on different dates [39].

To our knowledge, the type 2 processing proposed in this paper has never been documented before. It provided relevant results for the sandy terrace, which is made of relatively homogeneous pixels. In contrast, the type 2 correction turned out to be inefficient in the fringing zone. This result may partly be explained by tide, which may affect Equations (3) and (4) with stronger intensity in the fringing area, shallower than the sandy terrace area. Moreover, the heterogeneity of the fringing area, which is a mix of sand, corals and seagrasses, may also contribute to the poor performance of type 2 correction. Indeed, pixel resampling and misregistration may affect the signal to a greater extent in this heterogeneous area than in the sandy area. Implementing a co-registration method to correct errors and align pixels between images could be beneficial for future case-studies when the habitat is highly heterogeneous.

4.3. Supervised vs. Unsupervised Approach

The supervised and unsupervised approaches tested in this study to hindcast the algal dynamics offer different levels of cost effectiveness. Concerning 'costs' (in terms of time and expertise), the unsupervised method only involves a quick QGIS manipulation of a few minutes per image and does not require any specific expertise. The supervised approach, by contrast, requires the capacity to identify the presence/absence of algal mats

on Sentinel-2 images, an expertise acquired by comparing field observations concurrent with images. The method also requires a longer analysis time (i.e., ~20 min per image for the PGD area). The cost depends on the surface area to process and can be significant for large lagoons. Although the unsupervised approach does not require any expertise (beside understanding the software), the processing time (using R software) associated to this approach increases exponentially with the number of pixels. For the entire PGD area (fringing zone and sandy terrace zone confounded, assembling 94,202 pixels), the algorithm takes about 1 h to complete (computer with 8192 Mo usable RAM and ~1.8 GHz processor). This may impair, for larger areas, the feasibility of real-time processing to anticipate beach stranding events. By contrast, following the interactive part, the processing time using R software associated to the supervised approach only takes a few minutes to complete, regardless of the size of the area, as it manipulates vectors (i.e., polygons) of several hectares instead of 100 m² pixels raster data.

Regarding the accuracy of estimations, the supervised approach allowed to discriminate the two bloom periods which led to beach stranding events in the PGD area. The unsupervised approach, by contrast, could not identify these specific events. The unsupervised approach also overestimated the average algal abundance (\bar{I}_a) over the study period (i.e., from 2017 to 2019). Indeed, the field survey carried out in November 2019 reported a fringing zone free of algae, while the algal abundance hindcasted on the reference image by the unsupervised approach was high (mean \bar{I}_a value equal to 2.39). The supervised approach, on the other hand, provided more plausible estimates ($\bar{I}_a = 0.53$ on 25 November 2019). We thus recommend the supervised approach over the unsupervised one when the time and level of expertise are not constrained.

4.4. Tracking the Origin of Green Tides

The abundance of green algae estimated using Sentinel-2 data enabled identifying a bloom of algae located in the fringing area before the beach stranding event reported at PGD in January 2018. Therefore, the hindcast of algal dynamics performed in this study provides clues to identify the main pathways of nutrients that induced this event. Indeed, to implement management actions, local stakeholders lacked evidence on whether the stranding event recorded at PGD in front of the fringing area was induced by an input of nutrients very locally or if it was the result of the drift of algae biomass that originated elsewhere. Here, we provide evidence of the existence of a peak of algal abundance on the fringing area starting several weeks before the beaching event. By contrast, the abundance hindcasted in the sandy terrace before the beach stranding event of 18 January 2018 is quite low ($\bar{I}_a < 1$ for both approaches, see Figure S2). These results suggest that this stranding event was mainly due to algae biomass from the fringing zone. This hypothesis is consistent with the identification of two distinct species of *Ulva* genus in the PGD lagoon, which respectively dominate the sandy terrace and the fringing area [27,28]. The morphology of the species dominating the fringing area (i.e., forming dense unattached mats of long filamentous thallus) is more likely to generate green tides compared to the species that dominates the sandy terrace (species forming a smaller thallus attached to the substratum) [27,28].

It is worth noting that to track the origin of green tides in the PGD lagoon, we here developed an approach slightly different than those implemented in previous remote sensing studies for monitoring green macroalgae proliferations. Indeed, as previous studies focused on floating algae while drifting on the ocean surface, they aimed at developing methods that can detect these mats across wide areas of oceanic waters [16–20]. By contrast, the framework developed here aimed at hindcasting algae abundance in small areas suspected to experience green tides. Although this new framework requires sufficient knowledge on suitable habitats for algae and potential sources of nutrient to identify a priori the area that will be monitored, it is more relevant for monitoring blooms in small lagoons, where the rafting phase before beaching can be very brief and very spatially restricted within the lagoon.

4.5. Predicting the Risk of Beach Stranding Events

This study reconstructed the dynamics of green algae almost continuously over a three-year period. Similar objectives are not possible from in situ data. Although the fringing zone in the PGD lagoon is quite small and easily accessible from the beach, monitoring green algae cover in situ on a regular basis and in the long run turned out to be difficult to implement in practice, and using remote sensing is an attractive option. Eventually, we provided an indicator of risk for beach stranding events based on the estimates of green algal abundance (\bar{I}_a), via the supervised approach, with a 5-day periodicity (assuming favorable cloud cover). The dynamics reconstructed in this study over the period 2017–2019, with two significant bloom periods, can be used to set threshold values for \bar{I}_a , beyond which appropriate management actions may be needed (Table 2). Notably, the beaching risk can be considered as null when \bar{I}_a in the fringing area is lower than 0.53, which is, as on 25 November 2019, the predicted value at the time of very low algal abundance confirmed in the field (Figure 3c). This baseline value, which is not equal to zero, corresponds to a background noise due to the various processing steps. Conversely, the beach stranding risk can be considered high when $1.13 < \bar{I}_a < 1.86$, thus, as in conditions observed in January 2018 and June 2019. In such cases, management actions can be preconceived to prevent and minimize the pile-up of algae on the beach (Table 2).

Table 2. Framework proposed in the context of Poé-Gouaro-Deva for linking the abundance of algae in the fringing area hind-casted with the supervised method (\bar{I}_a) with management actions. The \bar{I}_a values are estimated from the θ_4 index, without any radiometric corrections.

\bar{I}_a Values	Beach Stranding Risk	Management Action Suggested
$I_a \leq 0.53$	Null	None
$0.53 \leq I_a \leq 0.95$	Low	None
$0.95 \leq I_a \leq 1.13$	Moderate	<ul style="list-style-type: none"> • Implementation of daily monitoring by an agent in situ
$1.13 \leq I_a \leq 1.86$	High	<ul style="list-style-type: none"> • Implementation of daily monitoring by an agent in situ • Launching/processing of clean-up operations on the beach
$1.86 \leq I_a$	Extreme	<ul style="list-style-type: none"> • Implementation of daily monitoring by an agent in situ • Check possible light obstruction for corals and seagrass and eventually consider launching field collection of macroalgae to reduce the threat for the ecosystem • Launching/processing of clean-up operations on the beach

Among the management actions that are recommended in case of moderate, high or extreme risk forecasted by the near real-time remote sensing protocol, we suggest (1) the implementation of, ideally, daily monitoring of algal cover along the fringing zone. This is recommended because the periodicity of the Sentinel-2 imagery (i.e., 5 days, assuming cloud-free weather) may be insufficient to accurately characterize the short-term evolution of each bloom. A second action recommended is (2) to plan clean-up measures on the beach. The removal of algae biomass accumulated along the shore is essential in order to avoid degradation of algae under anaerobic conditions and release of hydrogen sulfide. Finally, a third action that could be considered here in case of extreme risk of stranding events is (3) to remove a significant amount of macroalgae from the areas propitious to their growth (e.g., through field collection) in order to slow down the growth of the population. Although this action has already proven its efficiency to get rid of an already-formed bloom of green macroalgae [9], it seems difficult to implement in the PGD fringing zone without significantly damaging the coral reef and seagrass habitats.

Despite that the Sentinel-2 missions are expected to end in 2024, the development of such an indicator of risk for beach stranding events using this imagery is a promising path for environmental management. Indeed, the ESA agency has mentioned a possible 5-year extension of their products with new satellites to be launched, thus ensuring an access

to Sentinel-2 imagery until 2029. Beyond the Sentinel-2 imagery, one can also expect the launch of new missions providing products at higher temporal and/or spatial resolution, which should also provide relevant data for monitoring green macroalgae blooms in shallow lagoons.

4.6. Generalization to Other Lagoons in New Caledonia

In this study we demonstrated the potential of using Sentinel-2 images to monitor green macroalgae proliferation in the PGD shallow lagoon. Statistical relationships established between the θ_4 radiometric index and the green algae abundances, as well as radiometric corrections recommended for this study, were zone-sensitive (Figures 5 and 6). Even though the shallow habitats, either fringing or part of the barrier reef complex, represent wide areas at the New Caledonia scale (Figure 1), the PGD lagoon is quite an uncommon feature in New Caledonia due to its shallow depth and geomorphology [29,31]. The optical signature of the bands may vary from one site to another, depending on various parameters, including bathymetry, substrate nature, benthic components other than macroalgae and water quality. The diversity of these features is high in New Caledonia, and more work is needed at other sites to test the robustness of the methods established here.

Specifically for water quality, performing water column correction was not justified in our study since phytoplankton blooms were of lower concern in the PGD lagoon. Indeed, considering the shallow depths (between ~1.5 and 4 m) and low chl-a concentration in our study area (from 0.17 mg.m^{-3} after a dry period to 0.75 mg.m^{-3} after a heavy rain event, unpublished data), the decay of light along the water column remains fairly acceptable for the blue and green bands [57]. Moreover, the spatial patterns of algae blooms that can be observed on the imagery followed the benthic features of the area (Figure 3), indicating that the measured optical changes were driven by benthic algae, not by phytoplankton blooms. Finally, among all the methods developed to date for water column correction, none are capable of completely eliminating the water column effect [57]. All methods require some inputs that were not available with sufficient accuracy in our study area, and some others make assumptions not supported in our study site. As a result, performing a water column correction with available data was likely to induce more bias in the analysis. Applying the framework developed for PGD to other sites may, however, require an additional step of water column correction, especially for lagoons characterized by higher chl-a concentration or deeper habitats than studied here. Note that such an additional step is not trivial, as it may require the acquisition of specific data for model input, including accurate depth or bathymetric maps, or high-resolution maps of substrate and knowledge on the spectral behavior of each substrate type [57].

5. Conclusions

The capacity of Sentinel-2 imagery to hindcast the dynamics of green algae in shallow lagoons has been demonstrated for the PGD lagoon. It is a promising tool to track down the origin of green tides and identify potential sources. In particular, this paper highlights that an updated version of the NDVI, based on the blue and the green spectral bands instead of the red and near-infrared ones, can quantify the abundance of benthic green algae. However, the accuracy of the estimates is sensitive to the type of corrections applied to the radiometric values and the type of substrate. This prevents the transferability of the method to other sites without field validation. For the reconstruction of algae dynamics over specific and short periods, a supervised approach is recommended since it provides more accurate estimations of algal abundance. Hindcasting the algal dynamics over the 2017–2019 period evidenced that the massive beach stranding event that occurred in January 2018 in the northwest part of the PGD lagoon was the result of a macroalgae bloom that took place locally in this area. Based on our results, an indicator has been proposed to monitor the risk of beach stranding in near real-time and assist coastal management.

Supplementary Materials: The following are available online at <https://www.mdpi.com/2072-4292/13/2/211/s1>, Figure S1: Calibration of a smooth function (non-parametric relationship) between the green algal abundance and the radiometric index NDVI using the red and near-infrared bands. Figure S2: Algal abundances located in the fringing zone vs. in the sandy terraces before the beach stranding event of 18 January 2018.

Author Contributions: Conceptualization, M.B., S.V.W. and S.A.; methodology, M.B. and S.V.W.; software, M.B., S.V.W. and E.B.; validation, S.V.W., S.A., C.P., R.L.G., B.S. and E.C.; formal analysis, M.B.; investigation, M.B. and S.V.W.; resources, E.C.; data curation, M.B.; writing—original draft preparation, M.B. and S.V.W.; writing—review and editing, S.A., C.P., B.S., E.B., R.L.G. and E.C.; visualization, M.B.; supervision, S.V.W.; project administration, M.B., S.V.W., B.S. and E.C.; funding acquisition, E.C., S.V.W. and B.S. All authors have read and agreed to the published version of the manuscript.

Funding: This research was funded by: Direction du développement durable des territoires, Province Sud, New Caledonia. Grant number C.458-19.

Data Availability Statement: The data presented in this study are openly available at [<https://sextant.ifremer.fr>].

Acknowledgments: We are grateful to Miguel Clarke, Alan Choupeau and Romain Laigle for their logistical support during field trips; to Siloë Gobin and Thierry Jauffrais for their help in collecting macroalgae during fieldwork and macroalgae identification. We also thank Laurent Millet, Clarisse Majorel and Claire Bonneville from the “Plateforme du vivant”, where genetic analyses were performed to support algae identification. We also thank the other members of the project that contributed to reviewing this work during workshops, including Hugues Lemonnier and Emmanuel Tessier.

Conflicts of Interest: The authors declare no conflict of interest.

References

- Ye, N.H.; Zhang, X.W.; Mao, Y.Z.; Liang, C.W.; Xu, D.; Zou, J.; Zhuang, A.M.; Wang, Q.Y. ‘Green tides’ are overwhelming the coastline of our blue planet: Taking the world’s largest example 1994. *Ecol. Res.* **2011**, *26*, 477–485. [[CrossRef](#)]
- Gladyshev, M.I.; Gubelit, Y.I. Green Tides: New Consequences of the Eutrophication of Natural Waters (Invited Review). *Contemp. Probl. Ecol.* **2019**, *12*, 109–125. [[CrossRef](#)]
- Piriou, J.Y.; Ménesguen, A. Les marées vertes à Ulves: Conditions nécessaires, évolution et comparaison de sites. IFREMER: Centre de Brest, BP 70, F-29263 Plouzané, France. Dans. *Estuaries Coasts Spat. Temporal. Intercomp.* **1991**, *19*, 117.
- Runca, E.; Bernstein, A.; Postma, L.; Di Silvio, G. Control of macroalgae blooms in the Lagoon of Venice. *Ocean Coast. Manag.* **1996**, *30*, 235–257.
- Flindt, M.R.; Kamp-Nielsen, L.; Marques, J.C.; Pardal, M.A.; Bocci, M.; Bendoricchio, G.; Salomonsen, J.; Nielsen, S.N.; Jorgensen, S.E. Description of the three shallow estuaries: Montego River (Portugal), Roskilde Fjord (Denmark) and the lagoon of Venice (Italy). *Ecol. Model.* **1997**, *102*, 17–31. [[CrossRef](#)]
- Hernandez, I.; Peralta, G.; Pérez-Llorés, J.L.; Vergara, J.J. Biomass and dynamics of growth of *Ulva* species in Palmones river estuary. *J. Phycol.* **1997**, *33*, 764–772.
- Liu, D.; Keesing, J.K.; Xing, Q.; Shi, P. World’s largest macroalgal bloom caused by expansion of seaweed aquaculture in China. *Mar. Pollut. Bull.* **2009**, *58*, 888–895. [[CrossRef](#)]
- Chávez-Sánchez, T.; Piñón-Gimate, A.; Serviere-Zaragoza, E.; López-Bautista, J.M.; Casas-Valdez, M. Ulva blooms in the southwestern Gulf of California: Reproduction and biomass. *Estuarine Coast. Shelf Sci.* **2018**, *200*, 202–211.
- Ménesguen, A. *Les Marées Vertes. 40 Clés Pour Comprendre*; Edition Quae: Versailles, France, 2018; p. 128.
- Wang, X.H.; Li, L.; Bao, X.; Zhao, L.D. Economic cost of an algae bloom cleanup in China’s 2008 Olympic sailing venue. *EosTrans. Am. Geophys. Union* **2009**, *90*, 238–239.
- Han, Q.; Liu, D. Macroalgae blooms and their effects on seagrass ecosystems. *J. Ocean Univ. China* **2014**, *13*, 791–798.
- Zhang, Y.; He, P.; Li, H.; Li, G.; Liu, J.; Jiao, F.; Zhang, J.; Huo, Y.; Shi, X.; Su, R.; et al. *Ulva prolifera* green-tide outbreaks and their environmental impact in the Yellow Sea, China. *Nat. Sci. Rev.* **2019**, *6*, 825–838.
- Santos, R.O.; Varona, G.; Avila, C.L.; Lirman, D.; Collado-Vides, L. Implications of macroalgae blooms to the spatial structure of seagrass seascapes: The case of the *Anadyomene* spp. (Chlorophyta) bloom in Biscayne Bay, Florida. *Mar. Pollut. Bull.* **2020**, *150*, 110742. [[CrossRef](#)] [[PubMed](#)]
- Scanlan, C.M.; Foden, J.; Wells, E.; Best, M.A. The monitoring of opportunistic macroalgal blooms for the water framework directive. *Mar. Pollut. Bull.* **2007**, *55*, 162–171. [[PubMed](#)]
- Perrot, T.; Rossi, N.; Ménesguen, A.; Dumas, F. Modelling green macroalgal blooms on the coasts of Brittany, France to enhance water quality management. *J. Mar. Syst.* **2014**, *132*, 38–53.

16. Qi, L.; Hu, C.; Xing, Q.; Shang, S. Long-term trend of *Ulva prolifera* blooms in the western Yellow Sea. *Harmful Algae* **2016**, *58*, 35–44. [[CrossRef](#)] [[PubMed](#)]
17. Qi, L.; Hu, C.; Wang, M.; Shang, S.; Wilson, C. Floating algae blooms in the East China Sea. *Geophys. Res. Lett.* **2017**, *44*, 501–509. [[CrossRef](#)]
18. Xing, Q.; Guo, R.; Wu, L.; An, D.; Cong, M.; Qin, S.; Li, X. High-resolution satellite observations of a new hazard of golden tides caused by floating *Sargassum* in winter in the Yellow Sea. *IEEE Geosci. Remote Sens. Lett.* **2017**, *14*, 1815–1819.
19. Gower, J.; Young, E.; King, S. Satellite images suggest a new *Sargassum* source region in 2011. *Remote Sens. Lett.* **2013**, *4*, 764–773. [[CrossRef](#)]
20. Zheng, H.; Liu, Z.; Chen, B.; Xu, H. Quantitative *Ulva Prolifera* bloom monitoring based on multi-source satellite ocean color remote sensing data. *Appl. Ecol. Environ. Res.* **2020**, *18*, 4897–4913.
21. Xing, B.; Li, J.; Zhu, H.; Wei, P.; Zhao, Y. Construction of green tide monitoring system and research on its key techniques. *Int. Arch. Photogramm. Remote Sens. Spat. Inform. Sci.* **2018**, *XLII-3*, 1963–1970.
22. Qiu, Z.; Li, Z.; Bilal, M.; Wang, S.; Sun, D.; Chen, Y. Automatic method to monitor floating macroalgae blooms based on multilayer perception: Case study of Yellow Sea using GOCI images. *Opt. Express* **2018**, *26*, 26810–26829. [[CrossRef](#)]
23. Jiang, B.; Fan, D.; Ji, Q.; Obodoefuna, D.C. Dynamic Diurnal Changes in Green Algae Biomass in the Southern Yellow Sea Based on GOCI Images. *J. Ocean Univ. China* **2020**, *19*, 811–817. [[CrossRef](#)]
24. Andréfouët, S.; Zubia, M.; Payri, C. Mapping and biomass estimation of the invasive brown algae *Turbinaria ornata* (Turner) J. Agardhand *Sargassum mangarevense* (Grunow) Setchell on heterogeneous Tahitian coral reefs using 4-meter resolution IKONOS satellite data. *Coral Reefs* **2004**, *23*, 26–38.
25. Hoang, T.C.; Cole, A.J.; Fotedar, R.K.; O’Leary, M.J.; Lomas, M.W.; Roy, S. Seasonal changes in water quality and *Sargassum* biomass in southwest Australia. *Mar. Ecol. Prog. Ser.* **2016**, *551*, 63–79. [[CrossRef](#)]
26. Andréfouët, S.; Payri, C.; Van Wynsberge, S.; Lauret, O.; Alefaio, S.; Preston, G.; Yamano, H.; Baudel, S. The timing and the scale of the proliferation of *Sargassum polycystum* in Funafuti Atoll, Tuvalu. *J. Appl. Phycol.* **2017**, *29*, 3097–3108. [[CrossRef](#)]
27. Gobin, S. Diversité Génétique et Morphologique des Ulves (Ulvophyceae, Chlorophyta) en Nouvelle-Calédonie. Master’s Thesis, Université de Nantes, Nantes, France, 2019; p. 39.
28. Lagourgue, L. Genetic and Morphological Diversity of Ulva (Ulvophyceae, Chlorophyta) in New Caledonia. In prep.
29. Andréfouët, S.; Cabioch, G.; Flamand, B.; Pelletier, B. A reappraisal of the diversity of geomorphological and genetic processes of New Caledonian coral reefs: A synthesis from optical remote sensing, coring and acoustic multibeam observations. *Coral Reefs* **2009**, *28*, 691–707. [[CrossRef](#)]
30. Gairin, E.; Andréfouët, S. Role of habitat definition on Aichi Target 11: Examples from New Caledonian coral reefs. *Mar. Policy* **2020**, *116*, 103951. [[CrossRef](#)]
31. Andréfouët, S.; Chagnaud, N.; Chauvin, C.; Kranenburg, C. *Atlas of the French Overseas Coral Reefs*; Centre IRD de Nouméa: Nouméa, New Caledonia, 2008; p. 154.
32. Observatoire de l’Environnement Nouvelle Calédonie. Available online: www.oeil.nc (accessed on 5 January 2021).
33. Andréfouët, S.; Wantiez, L. Characterizing the diversity of coral reef habitats and fish communities found in a UNESCO World Heritage Site: The strategy developed for Lagoons of New Caledonia. *Mar. Pollut. Bull.* **2010**, *61*, 612–620. [[CrossRef](#)]
34. Pleiades | Le Site du Centre National d’Etudes Spatiales. Available online: <https://pleiades.cnes.fr/fr> (accessed on 5 January 2021).
35. Braun-Blanquet, J. *Plant. Sociology (Translation Fuller. GD and Conrad HS)*; McGrax-Hill: New York, NY, USA, 1932; p. 539.
36. Copernicus Open Access Hub. Available online: www.scihub.copernicus.eu (accessed on 5 January 2021).
37. Clua, E.; Legendre, P.; Vigliola, L.; Magron, F.; Kulbicki, M.; Sarramegna, S.; Labrosse, P.; Galzin, R. Medium scale approach (MSA) for improved assessment of coral reef fish habitat. *J. Exp. Mar. Biol. Ecol.* **2006**, *333*, 219–230. [[CrossRef](#)]
38. Hochberg, E.J.; Peltier, S.A.; Maritorena, S. Trends and variability in spectral diffuse attenuation of coral reef water. *Coral Reefs* **2020**, *39*, 1377–1389.
39. Andréfouët, S.; Muller-Karger, F.; Hochberg, E.; Hu, C.; Carder, K. Change detection in shallow coral reef environments using Landsat 7 ETM+ data. *Remote Sens. Environ.* **2001**, *79*, 150–162. [[CrossRef](#)]
40. Baret, F.; Guyot, G. Potentials and limits of vegetation indices for LAI and APAR assessment. *Remote Sens. Environ.* **1991**, *35*, 161–173.
41. Tucker, C.J. Red and photographic infrared linear combinations for monitoring vegetation. *Remote Sens. Environ.* **1979**, *8*, 127–150. [[CrossRef](#)]
42. Fassnacht, K.S.; Gower, S.T.; MacKenzie, M.D.; Nordheim, M.D.; Lillesand, T.M. Estimating the leaf area index of north central Wisconsin forests using the Landsat thematic mapper. *Remote Sens. Environ.* **1997**, *61*, 229–245. [[CrossRef](#)]
43. Chen, J.M. Evaluation of vegetation indices and a modified simple ratio for boreal applications. *Can. J. Remote Sens.* **1996**, *22*, 229–242. [[CrossRef](#)]
44. Gong, P.; Pu, R.; Biging, G.S.; Larrieu, M.R. Estimation of forest leaf area index using vegetation indices derived from Hyperion hyperspectral data. *IEEE Trans. Geosci. Remote Sens.* **2003**, *41*, 1355–1362.
45. Kiage, L.M.; Walker, N.D. Using NDVI from MODIS to monitor duckweed bloom in Lake Maracaibo, Venezuela. *Water Resour. Manag.* **2009**, *23*, 1125–1135.
46. Villa, P.; Mousivand, A.; Bresciani, M. Aquatic vegetation indices assessment through radiative transfer modeling and linear mixture simulation. *Int. J. Appl. Earth Obs. Geoinf.* **2014**, *30*, 113–127. [[CrossRef](#)]

47. Pu, R.; Bell, S.; English, D. Developing hyperspectral vegetation indices for identifying seagrass species and cover classes. *J. Coast. Res.* **2015**, *31*, 595–615. [[CrossRef](#)]
48. Qing, S.; Runa, A.; Shun, B.; Zhao, W.; Bao, Y.; Hao, Y. Distinguishing and mapping of aquatic vegetations and yellow algae bloom with Landsat satellite data in a complex shallow Lake, China during 1986–2018. *Ecol. Indic.* **2020**, *112*, 106073. [[CrossRef](#)]
49. Visitacion, M.R.; Alnin, C.A.; Ferrer, M.R.; Suñiga, L. Detection of algal bloom in the coastal waters of Boracay, Philippines, using normalized difference vegetation index (NDVI) and floating algae index (FAI). *Int. Arch. Photogramm. Remote Sens. Spat. Inform. Sci.* **2019**, *XLII-4*, 8. [[CrossRef](#)]
50. Hu, C.; He, M.X. Origin and offshore extent of floating algae in Olympic sailing area. *EosTrans. Am. Geophys. Union* **2008**, *89*, 302–303. [[CrossRef](#)]
51. Valle, M.; Palà, V.; Lafon, V.; Dehouck, A.; Garmendia, J.M.; Borja, Á.; Chust, G. Mapping estuarine habitats using airborne hyperspectral imagery, with special focus on seagrass meadows. *Estuar. Coast. Shelf Sci.* **2015**, *164*, 433–442. [[CrossRef](#)]
52. Armstrong, R.A. Remote sensing of submerged vegetation canopies for biomass estimation. *Int. J. Remote Sens.* **1993**, *14*, 621–627. [[CrossRef](#)]
53. Dierssen, H.M.; Chlus, A.; Russell, B. Hyperspectral discrimination of floating mats of seagrass wrack and the macroalgae *Sargassum* in coastal waters of Greater Florida Bay using airborne remote sensing. *Remote Sens. Environ.* **2015**, *167*, 247–258. [[CrossRef](#)]
54. Yang, D.; Yang, C. Detection of seagrass distribution changes from 1991 to 2006 in Xincun Bay, Hainan, with satellite remote sensing. *Sensors* **2009**, *9*, 830–844. [[CrossRef](#)]
55. Lyons, M.; Phinn, S.; Roelfsema, C. Integrating Quickbird multi-spectral satellite and field data: Mapping bathymetry, seagrass cover, seagrass species and change in Moreton Bay, Australia in 2004 and 2007. *Remote Sens.* **2011**, *3*, 42–64.
56. Ilori, C.O.; Pahlevan, N.; Knudby, A. Analyzing performances of different atmospheric correction techniques for Landsat 8: Application for coastal remote sensing. *Remote Sens.* **2019**, *11*, 469. [[CrossRef](#)]
57. Zoffoli, M.L.; Frouin, R.; Kampel, M. Water column correction for coral reef studies by remote sensing. *Sensors* **2014**, *14*, 16881–16931. [[CrossRef](#)]